ADVANCED FUNCTIONAL MATERIALS
www.afm-journal.de

Highly Efficient Simple-Structure Blue and All-Phosphor Warm-White Phosphorescent Organic Light-Emitting Diodes Enabled by Wide-Bandgap Tetraarylsilane-Based Functional Materials

Shaolong Gong, Ning Sun, Jiajia Luo, Cheng Zhong, Dongge Ma, Jingui Qin, and Chuluo Yang**

Two host materials of {4-[diphenyl(4-pyridin-3-ylphenyl)silyl]phenyl}diphenylamine (*p*-PySiTPA) and {4-[[4-(diphenylphosphoryl)phenyl](diphenyl)silyl]phenyl}diphenylamine (*p*-POSiTPA), and an electron-transporting material of [(diphenylsilanediyl)bis(4,1-phenylene)]bis(diphenylphosphine) dioxide (SiDPO) are developed by incorporating appropriate charge transporting units into the tetraarylsilane skeleton. The host materials feature both high triplet energies (ca. 2.93 eV) and ambipolar charge transporting nature; the electron-transporting material comprising diphenylphosphine oxide units and tetraphenylsilane skeleton exhibits a high triplet energy (3.21 eV) and a deep highest occupied molecular orbital (HOMO) level (-6.47 eV). Using these tetraarylsilane-based functional materials results in a high-efficiency blue phosphorescent device with a three-organic-layer structure of 1,1-bis[4-[*N*,*N*-di(*p*-tolyl)-amino]phenyl]cyclohexane (TAPC)/*p*-POSiTPA: iridium(III) bis(4′,6′-difluorophenylpyridinato)tetrakis(1-pyrazolyl)borate (FIr6)/SiDPO that exhibits a forward-viewing maximum external quantum efficiency (EQE) up to 22.2%. This is the first report of three-organic-layer FIr6-based blue PhOLEDs with the forward-viewing EQE over 20%, and the device performance is among the highest for FIr6-based blue PhOLEDs even compared with the four or more than four organic-layer devices. Furthermore, with the introduction of bis(2-(9,9-diethyl-9*H*-fluoren-2-yl)-1-phenyl-1*H*-benzoimidazol-*N*,C^3) iridium acetylacetonate [$(fbi)_2Ir(acac)$] as an orange emitter, an all-phosphor warm-white PhOLED achieves a peak power efficiency of 47.2 lm W^{-1}, which is close to the highest values ever reported for two-color white PhOLEDs.

1. Introduction

High-efficiency organic light-emitting diodes (OLEDs) have generated considerable interests because of their bright future for the next-generation flat-panel displays and lighting sources.[1–3] In particular, phosphorescent OLEDs (PhOLEDs) have shown great potentials due to their merit of higher quantum efficiency compared with fluorescent OLEDs by utilizing both singlet and triplet excitons.[4–6] Among monochromatic PhOLEDs, the lack of efficient and stable blue PhOLEDs has become a major bottleneck to the development of efficient and stable white PhOLEDs, and thus restricts the commercialization of PhOLEDs in lighting sources. In comparision with sky-blue PhOLEDs based on the widely used phosphor of iridium(III) bis(4,6-(difluorophenyl)pyridine-*N*,$C^{2'}$) picolinate (FIrpic),[7] a blue PhOLED with a deeper blue emission shows more promise in reducing power consumption and improving color rendering index for illumination.[8] Until now, iridium(III) bis(4′,6′-difluorophenylpyridinato) tetrakis(1-pyrazolyl)borate (FIr6)[9–12] is still one of the typical phosphors for highly efficient PhOLEDs with a deeper blue emission. For example, a high-efficiency FIr6-based blue PhOLED with a peak external quantum efficiency (EQE) of 22.9% was fabricated by introducing *N*,*N*′-dicarbazolyl-3,5-benzene (*m*CP):*m*-bis(triphenylsilyl)benzene (UGH3) co-host system into the emitting layer;[10a] a maximum EQE of 20% was achieved by the FIr6-based blue PhOLED with the incorporation of a double emissive layer into the p-i-n device structure.[12b]

Dr. S. Gong, J. Luo, Dr. C. Zhong, Prof. J. Qin, Prof. C. Yang
Hubei Collaborative Innovation Center for Advanced Organic Chemical Materials
Hubei Key Lab on Organic and Polymeric Optoelectronic Materials
Department of Chemistry, Wuhan University
Wuhan 430072, PR China
E-mail: clyang@whu.edu.cn

N. Sun, Prof. D. Ma
State Key Laboratory of Polymer Physics and Chemistry
Changchun Institute of Applied Chemistry
Chinese Academy of Sciences
Changchun 130022, PR China
E-mail: mdg1014@ciac.jl.cn

DOI: 10.1002/adfm.201400149

Although gains in high EQEs are realized through the careful device optimization and material selection, at least four organic layers are required for almost all FIr6-based PhOLEDs with high efficiencies.[9–12] Except for typical three functional layers, that is the emitting layer (EML), hole- and electron-transporting layers (HTL and ETL), more layers are imperative to facilitate charge injection, transporting or blocking in the devices, which complicate the device structures and inevitably cause high operating voltages and increased manufacturing costs. Therefore, further effort on simplifying device structure while maintaining high device efficiency is highly desirable to make low-cost manufacturability amenable to commercial interests. However, the examples that can achieve satisfactory device performance in a simple device configuration remain rare.[13] This is mainly due to the lack of suitable functional materials to ensure charge balance and exciton confinement inside the EML in a simple device structure. The most critical problem to reach this goal is how to systematically manipulate the singlet and triplet energy levels as well as charge transporting properties of these functional materials used in HTL, ETL and EML. These functional materials should all have higher triplet energies (E_T) than 2.72 eV[14] of FIr6 to enable effective exciton confinement inside the EML. Besides this common requirement, one also expects the host materials to have ambipolar charge transporting nature to maximize the radiative recombination of carriers in the EML, and suitable highest occupied molecular orbital (HOMO) and lowest unoccupied molecular orbital (LUMO) levels to match with the adjacent HTL and/or ETL, thus benefiting hole and/or electron injection into the EML.[6a,15] For the HTL and ETL, the typical HTL of 1,1-bis[4-[*N*,*N*-di(*p*-tolyl)-amino]phenyl]cyclohexane (TAPC) has been widely used in blue PhOLEDs because of its high E_T (2.87 eV)[16] and good HT ability;[10,12,13] in contrast, excellent ET materials with sufficiently high triplet energies (>2.72 eV) to block exciton leakage are relatively unexplored.[17] Furthermore, it is desirable that ET materials possess deep HOMO level to act as a hole-blocking layer (HBL) in terms of the simplification of device structure. Therefore, the development of suitable host and ET materials remains a molecular designing challenge in efforts to realize high-efficiency blue PhOLEDs with simple device structure.

Our previous works demonstrated a series of tetraarylsilane-based host materials with both relatively high triplet energies and ambipolar transporting properties for sky-blue PhOLEDs, which achieved good performance in four-organic-layer devices.[18] In this work, we develop a series of wide-bandgap functional materials by incorporating suitable charge-transporting groups into the tetraarylsilane structure, that is, two host materials of *p*-PySiTPA and *p*-POSiTPA, and an ET material of SiDPO. The incorporation of electron-donor and -acceptor units into the tetraphenylsilane skeleton provides the host materials with high triplet energies (ca. 2.93 eV) and ambipolar charge transporting nature; the introduction of diphenylphosphine oxide acceptor into tetraphenylsilane structure endows the ET material with a high E_T (3.21 eV) and a deep HOMO level (–6.47 eV). Consequently, a high-efficiency blue phosphorescent device with a three-organic-layer structure of TAPC/*p*-POSiTPA:FIr6/SiDPO has been realized with a forward-viewing maximum EQE up to 22.2%. To the best of our knowledge, this is the first report of three-organic-layer FIr6-based blue PhOLEDs with the forward-viewing EQE over 20%. Furthermore, with the introduction of bis(2-(9,9-diethyl-9*H*-fluoren-2-yl)-1-phenyl-1*H*-benzoimidazol-*N*,C^3)iridium acetylacetonate [$(fbi)_2Ir(acac)$] as an orange emitter, an all-phosphor warm-white PhOLED has been realized with a peak power efficiency of 47.2 lm W^{-1}, which is close to the highest values ever reported for two-color white PhOLEDs.

2. Results and Discussion

2.1. Synthesis and Characterization

Scheme 1 depicts the synthetic routes and structures of {4-[diphenyl(4-pyridin-3-ylphenyl)silyl]phenyl}diphenylamine (*p*-PySiTPA), {4-[[4-(diphenylphosphoryl)phenyl](diphenyl)silyl]phenyl}diphenylamine (*p*-POSiTPA), and [(diphenylsilanediyl)bis(4,1-phenylene)]bis(diphenylphosphine) dioxide (SiDPO). Lithiation of **1** with n-butyllithium and subsequent treatment with excess diiodine afforded the intermediate **2**. The C-N coupling reaction of **2** with diphenylamine yielded the key intermediate **3**. *p*-PySiTPA was then synthesized by the Suzuki cross-coupling reaction of **3** with pyridin-3-ylboronic acid; whereas *p*-POSiTPA and SiDPO were prepared through a three-step procedure of lithiation, phophorization and oxidation from **3** and **1**, respectively. ^1H and ^{13}C NMR spectroscopies, mass spectrometry and elemental analysis (see the Experimental Section) were used to characterize the structures of these compounds.

2.2. Photophysical Properties

Figure 1 shows the UV-vis absorption, fluorescence and phosphorescence spectra of the compounds, and **Table 1** summrizes the key parameters. The optical bandgaps (E_g) of *p*-PySiTPA, *p*-POSiTPA, and SiDPO are estimated as 3.40, 3.41 and 4.26 eV, respectively, from the absorption edge of the films (Supporting Information Figure S1). The highest-energy vibronic sub-band of their phosphorescence spectra at 77 K (Figure 1 and Supporting Information Figure S2) have allowed us to determine the E_T of these compounds (2.92 eV for *p*-PySiTPA, 2.93 eV for *p*-POSiTPA and 3.21 eV for SiDPO). The higher E_T of the compounds than 2.72 eV of FIr6 could enable good exciton confinement on the blue phosphor FIr6. The suitability of *p*-PySiTPA and *p*-POSiTPA to host FIr6 are evaluated by measuring the photoluminescence quantum yields (PLQYs) of the films which comprise 10 wt% FIr6 in *p*-PySiTPA and *p*-POSiTPA, respectively. The relatively high PLQYs (86.5% for *p*-PySiTPA:10 wt% FIr6 and 86.8% for *p*-POSiTPA:10 wt% FIr6) are achieved for the doped films, which are slightly lower than the PLQY (96%) of FIr6 in dichoroethane solution.[19] Considering an accepted value for the light outcoupling efficiency of 25–30% and the excellent charge balance achieved in FIr6-based PhOLEDs, the maximum EQE of 22–26% is estimated for *p*-PySiTPA or *p*-POSiTPA:10 wt% FIr6 PhOLEDs, suggesting that *p*-PySiTPA and *p*-POSiTPA are potentially good hosts for FIr6.

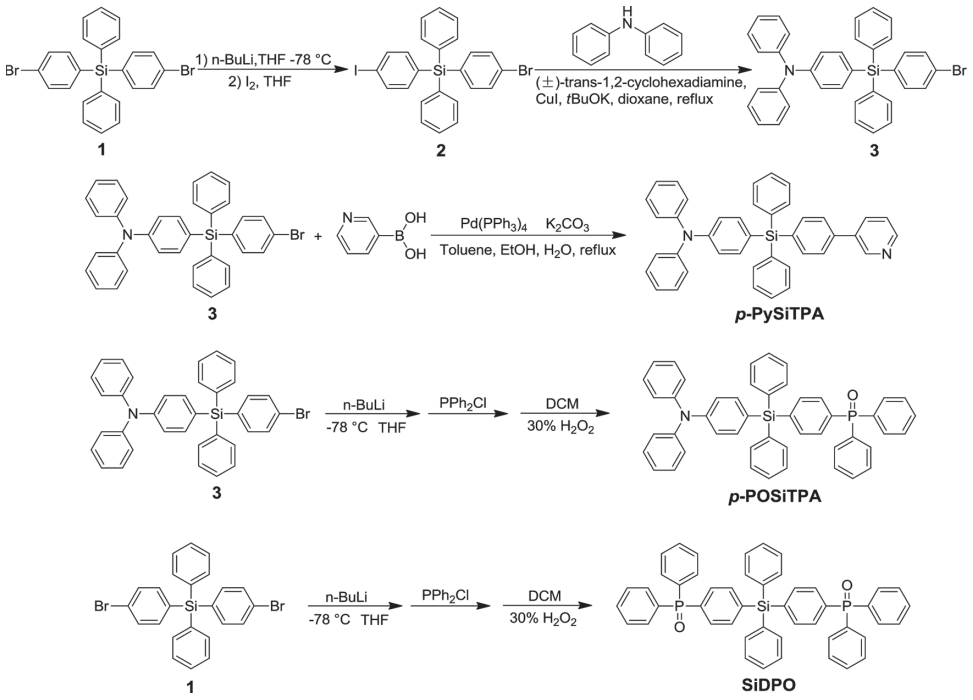

Scheme 1. Synthetic routes and structures of *p*-PySiTPA, *p*-POSiTPA, and SiDPO.

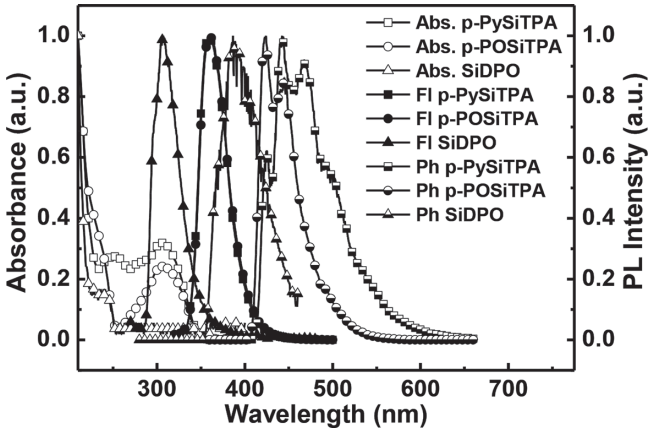

Figure 1. UV-vis absorption and fluorescence spectra of *p*-PySiTPA, *p*-POSiTPA, and SiDPO in hexane at 5×10^{-6} M at room temperature, and phosphorescence spectra of *p*-PySiTPA, *p*-POSiTPA, and SiDPO in 2-methyltetrahydrofuran at 77 K.

2.3. Thermal Properties and Film-Forming Ability

The thermal properties of *p*-PySiTPA, *p*-POSiTPA and SiDPO were investigated by the thermogravimetric analysis (TGA) and the differential scanning calorimetry (DSC) (**Figure 2** and Table 1). The decomposition temperatures (T_d, corresponding to 5% weight loss) are 384, 406 and 476 °C for *p*-PySiTPA, *p*-POSiTPA and SiDPO, respectively. These compounds show relatively high glass transition temperatures (T_g) of 71 (*p*-PySiTPA), 94 (*p*-POSiTPA) and 105 °C (SiDPO), which are higher than those of previously reported tetraarylsilane compounds (26–53 °C).[14] The good thermal performance could improve stability of film morphology and reduce possibility of phase separation upon heating. As shown in **Figure 3**, the atomic force microscopy (AFM) images of *p*-PySiTPA and *p*-POSiTPA films doped with FIr6 display smooth and homogeneous film morphologies, with the small values of root-mean-square (RMS) roughness at 0.24 and 0.21 nm. This indicates that the silicon tetrahedral configuration can provide

Table 1. Physical Properties of *p*-PySiTPA, *p*-POSiTPA, and SiDPO

compound	T_g [°C][a)]	T_d [°C][b)]	λ_{abs} [nm][c)]	$\lambda_{em,max}$ [nm][c)]	HOMO [eV][d)]	LUMO [eV][e)]	E_g [eV][f)]	E_T [eV][g)]
p-PySiTPA	71	384	252, 306	359	–5.32	–1.92	3.40	2.92
p-POSiTPA	94	406	307	360	–5.33	–1.92	3.41	2.93
SiDPO	105	476	241	307	–6.47	–2.21	4.26	3.21

[a)]Obtained from DSC measurements; [b)]Obtained from TGA measurements; [c)]Measured in hexane; [d)]Determined from the onset of oxidation potentials; [e)]Calculated from HOMO and E_g; [f)]Determined from the onset of absorption in film state; [g)]Measured in 2-methyltetrahydrofuran at 77 K.

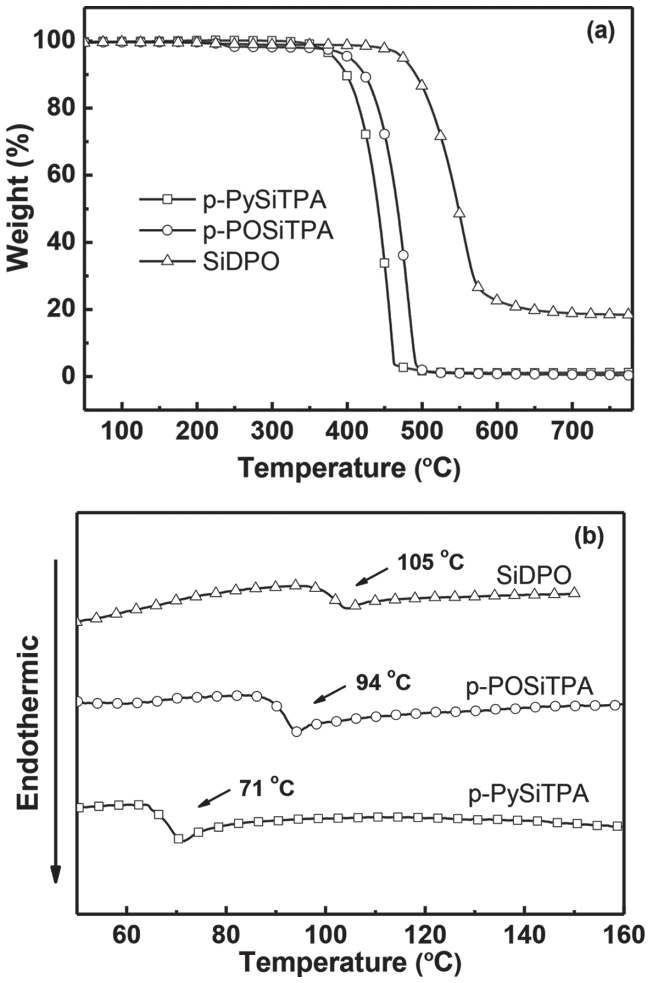

Figure 2. (a) TGA traces of *p*-PySiTPA, *p*-POSiTPA, and SiDPO recorded at a heating rate of 10 °C min^{-1}. (b) DSC traces of *p*-PySiTPA, *p*-POSiTPA, and SiDPO recorded at a heating rate of 10 °C min^{-1}.

a stabilizing environment for dopants and keep films integrity throughout the entire fabrication process.

2.4. Electrochemical Properties

Cyclic voltammetry (CV) were performed to investigate the electrochemical properties of the compounds. *p*-PySiTPA and *p*-POSiTPA exhibit one quasi-reversible, one-electron oxidation process (**Figure 4**a), which can be assigned to the oxidation of arylamine moiety.[20] The HOMO levels of *p*-PySiTPA and *p*-POSiTPA are –5.32 and –5.33 eV with regard to the energy level of ferrocene (–4.8 eV below vacuum), respectively, which well match to the HOMO level (–5.5 eV) of TAPC because of no hole-injection barriers from TAPC to these hosts.[21] SiDPO exhibits negligible oxidation signal during the anodic scan in dichloromethane or dimethylformamide. The LUMO level of SiDPO is –2.21 eV (Figure 4b), which can facilitate electron-injection into the EML. Its HOMO level estimated from the bandgap of SiDPO (4.26 eV) and LUMO is –6.47 eV, indicative of the potential utilization of SiDPO as an HBL/ETL.

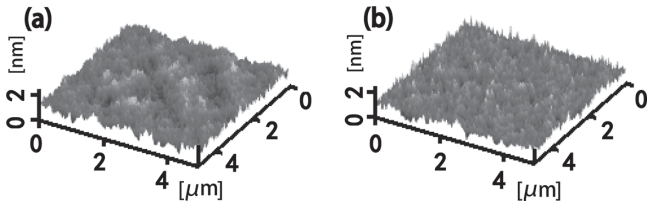

Figure 3. AFM images of the doped films prepared by vacuum thermal deposition with 10 wt% FIr6 in (a) *p*-PySiTPA and (b) *p*-POSiTPA.

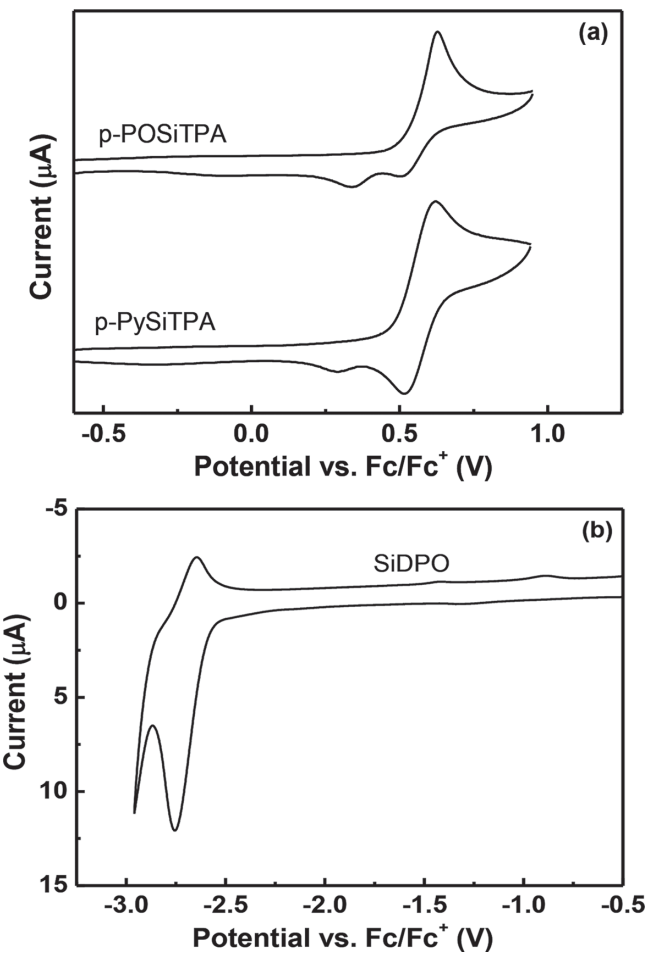

Figure 4. Cyclic voltammogram of (a) *p*-PySiTPA and *p*-POSiTPA in CH_2Cl_2 for oxidation scan, and (b) SiDPO in THF for reduction scan.

2.5. Electroluminescent Devices

To evaluate the performance of the newly-designed functional materials in blue PhOLEDs, two types of device structures were fabricated (**Figure 5**). The control devices (F1 and F2) have four-organic-layer structure of ITO/MoO_3 (10 nm)/TAPC (60 nm)/*p*-PySiTPA or *p*-POSiTPA: FIr6 (10 wt%, 20 nm)/1,3,5-tri(*m*-pyrid-3-yl-phenyl)benzene (Tm3PyPB, 5 nm)/1,3,5-tris(*N*-phenylbenzimidazol-2-yl)benzene (TPBI, 30 nm)/LiF (1 nm)/Al (100 nm). The simplified devices (T1 and T2) have three-organic-layer structure of ITO/MoO_3 (10 nm)/TAPC

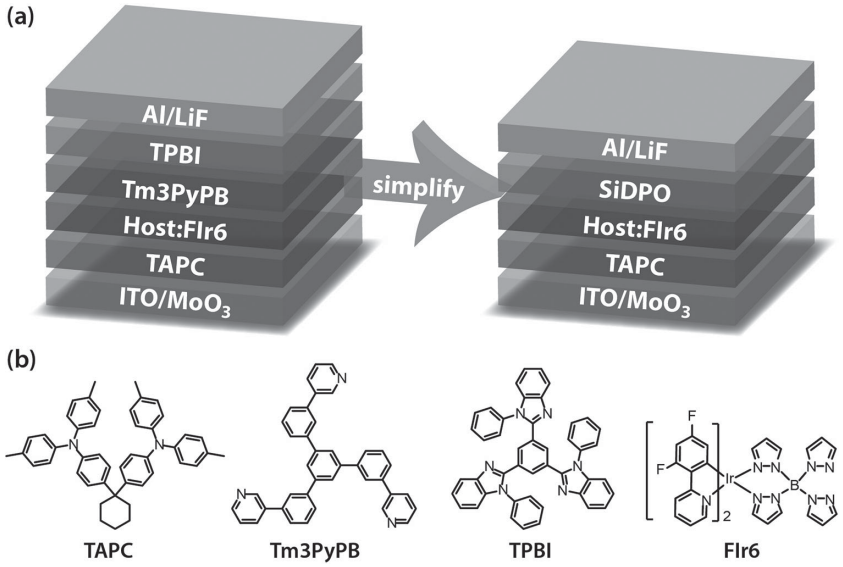

Figure 5. (a) Schematic of two type device structures of blue PhOLEDs. (b) Chemical structures of materials used for fabrication of devices.

(60 nm)/*p*-PySiTPA or *p*-POSiTPA: FIr6 (10 wt%, 20 nm)/SiDPO (35 nm)/LiF (1 nm)/Al (100 nm), where SiDPO acts as the HBL/ETL to replace Tm3PyPB[22] and TPBI[23] in control devices. MoO_3 and LiF serve as hole- and electron-injecting layers, respectively; TAPC functions as the HTL; FIr6 doped in *p*-PySiTPA or *p*-POSiTPA is utilized as EML, respectively.

Figure 6 shows the current density-voltage-luminance (*J-V-L*) characteristics and efficiency versus luminance curves for the devices, and **Table 2** summarizes the key device performance parameters. All the devices exhibit relatively low turn-on voltages (V_{on}, recorded at the luminance of 1 cd m^{-2}) in the range of 3.1–3.3 V, which can be rationalized by the well-matched HOMO levels of *p*-PySiTPA and *p*-POSiTPA with the HTL of TAPC. Noticablely, the simplified three-organic-layer devices T1 and T2 exhibit much higher efficiencies than the control four-organic-layer devices F1 and F2, respectively. For instance, the *p*-PySiTPA-based device T1 achieves a maximum current efficiency (CE_{max}) of 33.5 cd A^{-1} (Supporting Information Figure S3), a maximum power efficiency (PE_{max}) of 34.0 lm W^{-1} and a maximum EQE (EQE_{max}) of 18.8%, which outperform those of the control device F1 (CE_{max} of 22.0 cd A^{-1}, PE_{max} of 15.7 lm W^{-1} and EQE_{max} of 12.4%). Furthermore, the *p*-POSiTPA-based simplified device T2 exhibits better performance than *p*-PySiTPA-based device T1, with the forward-viewing CE_{max} of 40.1 cd A^{-1}, PE_{max} of 40.5 lm W^{-1} and EQE_{max} of 22.2%. Similarly, *p*-POSiTPA-based device F2 displays substantially higher efficiencies (CE_{max} of 25.9 cd A^{-1}, PE_{max} of 20.8 lm W^{-1} and EQE_{max} of 13.8%) than *p*-PySiTPA-based device F1. These results indicates the superiority of host material *p*-POSiTPA over *p*-PySiTPA. Given the fact that the doped films exhibit almost the same PLQYs (86.5% for *p*-PySiTPA:10 wt% FIr6 and 86.8% for *p*-POSiTPA:10 wt% FIr6), the origin of the different device performance could be the discrepancy in charge balance of *p*-PySiTPA and *p*-POSiTPA in FIr6-based devices. Remarkably, device T2 shows rather low efficiency roll-off: at the luminance of 100 cd m^{-2}, EQE is still up to 21.5% with a efficiency roll-off value of only 3.2%; even at the high luminance of 1000 cd m^{-2}, EQE remains as high as 17.1%. We have summarized the EL performance of representative FIr6-based PhOLEDs in **Table 3**. There are few examples reported in the literature on three-organic-layer FIr6-based blue PhOLEDs: Xue et al. reported a three-organic-layer FIr6-based blue PhOLED with EQE_{max} of only 5.5% in the structure of TAPC/UGH2:FIr6/BCP;[9b] Fukagawa et al. demonstrated PE_{max} of 19 lm W^{-1} and EQE_{max} of 14% in the structure of TAPC/Ad-CzPd:FIr6/TmPyPB.[13] To the best of our knowledge, this work is the first report of three-organic-layer FIr6-based blue PhOLEDs with the forward-viewing EQE above 20%, and the device performance is among the highest for FIr6-based blue PhOLEDs even compared with the four or more than four organic-layer devices.[10–12] We observed that the device luminescence went off after *ca.* 3 hours without encapsulation. The short lifetime of blue phosphorescent OLEDs are generally believed to result from the instability of blue phosphorescent iridium complexes.[24]

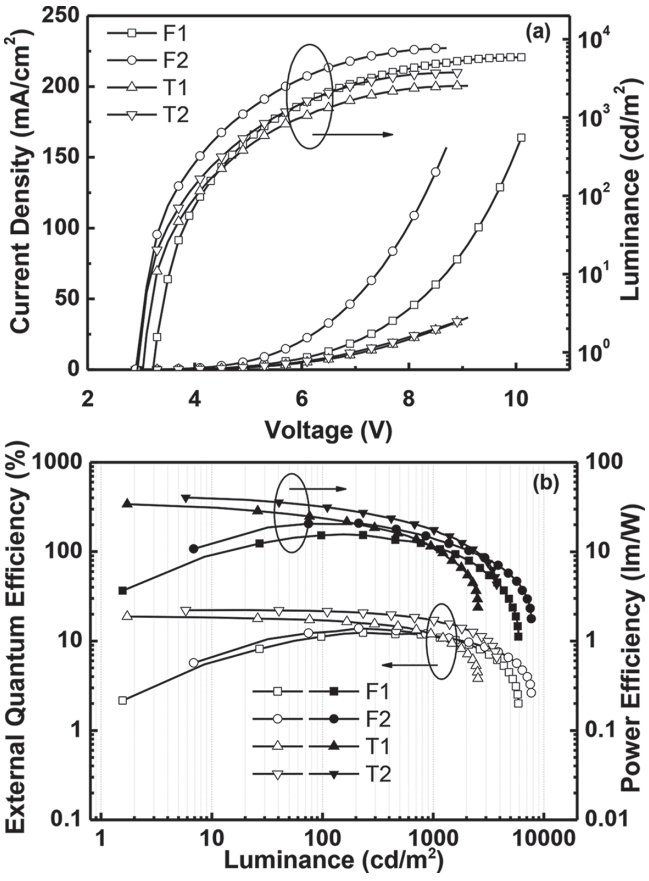

Figure 6. (a) Current density-voltage-luminance characteristics for devices F1, F2, T1 and T2. (b) External quantum efficiency and power efficiency versus luminance curves for devices F1, F2, T1 and T2.

Table 2. Summary of EL Performances (Forward-Viewing) of the Devices[a)]

device	host	HBL/ETL	V_{on} [V]	CE [cd A^{-1}][b)]	PE [lm W^{-1}][b)]	EQE [%][b)]	CIE [x, y][c)]
F1	*p*-PySiTPA	Tm3PyPB/TPBI	3.3	22.0, 19.9, 20.7	15.7, 15.2, 11.8	12.4, 11.2, 11.6	(0.15, 0.23)
F2	*p*-POSiTPA	Tm3PyPB/TPBI	3.1	25.9, 24.0, 21.1	20.8, 20.4, 13.5	13.8, 12.9, 11.3	(0.15, 0.24)
T1	*p*-PySiTPA	SiDPO	3.1	33.5, 30.2, 21.7	34.0, 23.1, 11.5	18.8, 16.9, 12.0	(0.15, 0.24)
T2	*p*-POSiTPA	SiDPO	3.1	40.1, 38.9, 30.7	40.5, 31.3, 17.5	22.2, 21.5, 17.1	(0.15, 0.24)
W1	*p*-PySiTPA	SiDPO	2.7	29.1, 24.7, 15.6	31.5, 22.2, 9.6	11.5, 9.8, 6.4	(0.45, 0.41)
W2	*p*-POSiTPA	SiDPO	3.1	46.5, 40.9, 27.3	47.2, 32.9, 15.6	18.7, 17.3, 11.3	(0.42, 0.42)

[a)]Abbreviations: HBL, hole-blocking layer; ETL, electron-transporting layer; V_{on}, turn-on voltage; CE, current efficiency; PE, power efficiency; EQE, external quantum efficiency; CIE [x, y], Commission International de l'Eclairage coordinates; [b)]Order of measured value: maximum, then values at 100 and 1000 cd m^{-2}; [c)]Measured at 7 V.

Table 3. EL Performance of Representative FIr6-Based PhOLEDs

reference	structure of organic layer	layer number	V_{on} [V]	CE_{max} [cd A^{-1}]	PE_{max} [lm W^{-1}]	EQE_{max} [%]	CIE [x, y]
this work	TAPC/*p*-POSiTPA:FIr6/SiDPO	three	3.1[a)]	40.1	40.5	22.2	(0.15, 0.24)
ref. [13]	TAPC/Ad-CzPd:FIr6/TmPyPB	three	3.6[a)]	-	19	14	(0.16, 0.26)
ref. [9b]	TAPC/UGH2:FIr6/BCP	three	-	-	7	5.5	–
ref. [10a]	TAPC/*m*CP:UGH3:FIr6/Tm3PyPB/Tm3PyPB:Cs	four	~3.2[a)]	39.5	39.2	22.9	(0.163, 0.287)
ref. [10b]	TAPC/TcTa:SPPO1:FIr6/Tm3PyPB/Tm3PyPB:Cs	four	-	-	43.5	20.5	–
ref. [11a]	NPB/*m*CP/BCPO:FIr6/TAZ	four	3.0[a)]	36.8	33.1	19.8	(0.14, 0.25)
ref. [11b]	NPB/*m*CP/BCPO:FIr6/*t*OXD-*m*TP	four	4.3[a)]	42.5	25.7	25.0	(0.14, 0.23)
ref. [12a]	TAPC/Ad-Cz:FIr6/Ad-Pd:FIr6/TPBI	four	3.2[b)]	-	33	19	(0.16, 0.28)
ref. [12b]	MeO-TPD:F_4-TCNQ/TAPC/*m*CP:FIr6/UGH2:FIr6/3TPYMB/3TPYMB:Cs	six	3.0[b)]	41	36	20	(0.16, 0.28)

[a)]Defined as the drive voltage at the luminance of 1 cd m^{-2}; [b)]Defined as the drive voltage at the luminance of 0.1 cd m^{-2}.

To determine the origin of the different device performance, we fabricated the hole-only devices with the structure of ITO/MoO_3 (10 nm)/TAPC (60 nm)/*p*-PySiTPA or *p*-POSiTPA (70 nm)/MoO_3 (10 nm)/Al, and two types of electron-only devices with the configurations of type A: Al/LiF (1 nm)/*p*-PySiTPA or *p*-POSiTPA (70 nm)/Tm3PyPB (5 nm)/TPBI (30 nm)/LiF (1 nm)/Al, and type B: Al/LiF (1 nm)/*p*-PySiTPA or *p*-POSiTPA (70 nm)/SiDPO (35 nm)/LiF (1 nm)/Al, corresponding to the control and simplified devices, respectively. MoO_3 and LiF layers are employed to prevent electron- and hole-injection from the cathode and anode, respectively. As shown in **Figure 7**, one can evaluate the electron/hole transporting balance for a compound by comparing the current densities under the same voltage between hole- and electron-only devices. Obviously, *p*-POSiTPA shows more balanced electron/hole transporting property over *p*-PySiTPA in both the control and simplified devices. On the other hand, the simplified devices employing SiDPO as ETL reveal more matched electron/hole transporting abilities than the control devices using Tm3PyPB/TPBI. The electron/hole transporting balance correlates well with the device efficiencies. We note that electron- and hole-only devices for *p*-POSiTPA with SiDPO as ETL show almost the same current densities under the same voltage, which could account for the best performance achieved by device T2 for the FIr6-based blue PhOLEDs.

In view of the success in the high-efficiency simple-structure blue PhOLEDs, we demonstrated two-color all-phosphor white PhOLEDs (devices W1 and W2) with the configuration of ITO/MoO_3 (10 nm)/TAPC (60 nm)/*p*-PySiTPA or *p*-POSiTPA: FIr6 (6 wt%, 7 nm)/*p*-PySiTPA or *p*-POSiTPA: $(fbi)_2Ir(acac)$ (8 wt%,

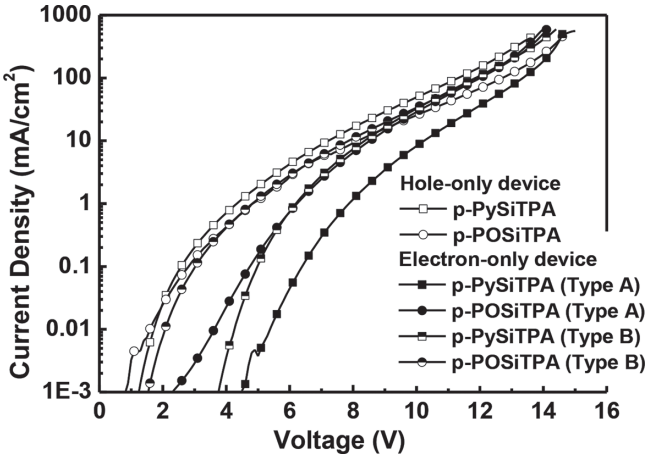

Figure 7. Current density versus voltage characteristics of the hole-only and electron-only devices. Hole-only devices: ITO/MoO_3 (10 nm)/TAPC (60 nm)/*p*-PySiTPA or *p*-POSiTPA (70 nm)/MoO_3 (10 nm)/Al. Electron-only devices: Al/LiF (1 nm)/*p*-PySiTPA or *p*-POSiTPA (70 nm)/Tm3PyPB (5 nm)/TPBI (30 nm)/LiF (1 nm)/Al (type A), and Al/LiF (1 nm)/*p*-PySiTPA or *p*-POSiTPA (70 nm)/SiDPO (35 nm)/LiF (1 nm)/Al (type B).

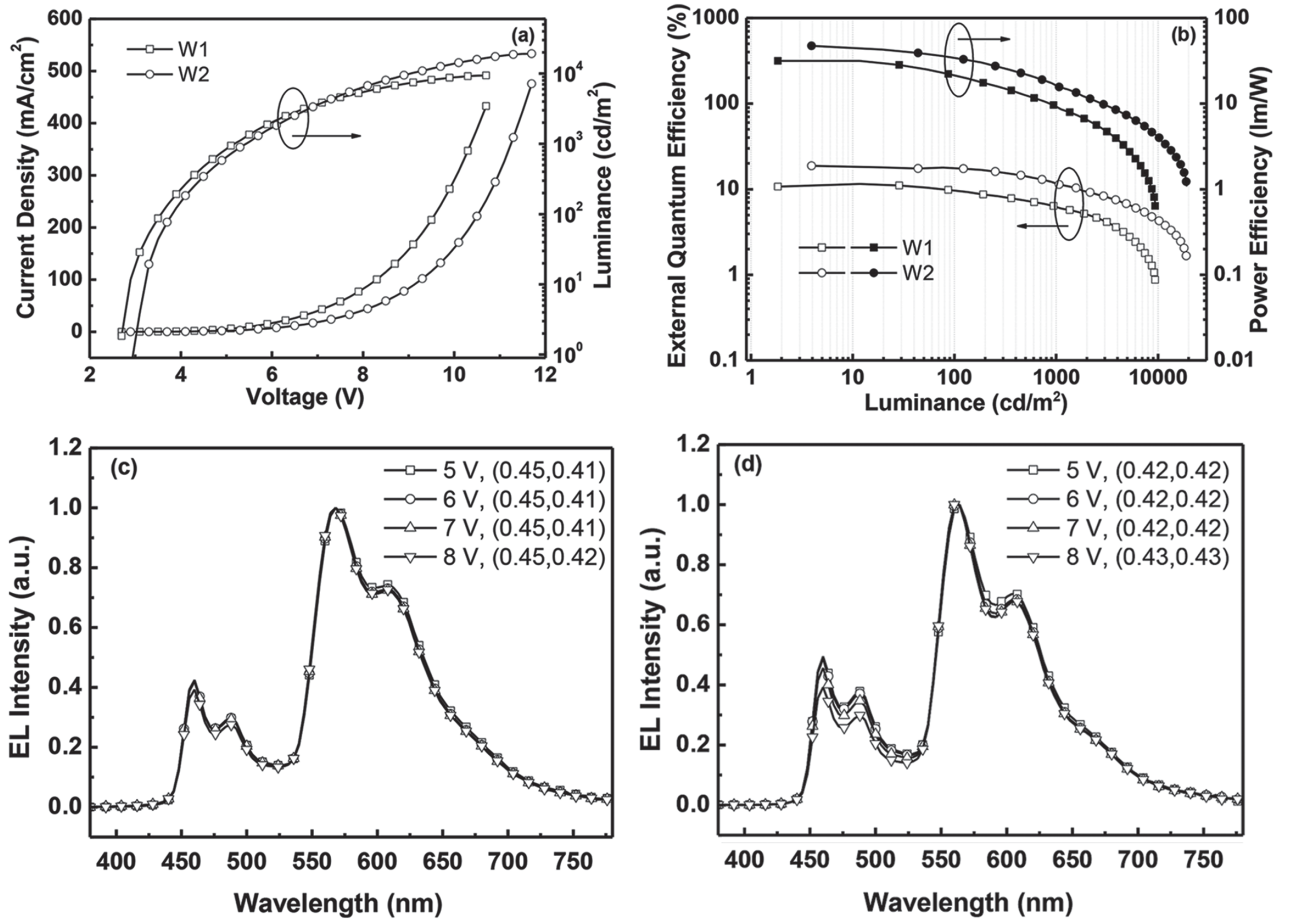

Figure 8. (a) Current density-voltage-luminance characteristics for devices W1 and W2. (b) External quantum efficiency and power efficiency versus luminance curves for devices W1 and W2. (c) The normalized EL spectra of device W1 at various voltages. (d) The normalized EL spectra of device W2 at various voltages.

10 nm)/SiDPO (35 nm)/LiF (1 nm)/Al (100 nm) through using bis(2-(9,9-diethyl-9*H*-fluoren-2-yl)-1-phenyl-1*H*-benzoimidazol-*N*,C^3)iridium acetylacetonate [$(fbi)_2Ir(acac)$] as an orange phosphor.[25] **Figure 8** shows the *J-V-L* characteristics, efficiency versus luminance curves, and the normalized EL spectra at various voltages for devices W1 and W2. Similar to the behavior of the blue devices, both white devices have relatively low V_{on} of 2.7 V for W1, and 3.1 V for W2. The *p*-PySiTPA-based device W1 shows a forward-viewing CE_{max} of 29.1 cd A^{-1} (Supporting Information Figure S4), PE_{max} of 31.5 lm W^{-1} and EQE_{max} of 11.5%. Furthermore, the *p*-POSiTPA-based device W2 exhibits better performance than *p*-PySiTPA-based device W1, with the CE_{max} of 46.5 cd A^{-1}, PE_{max} of 47.2 lm W^{-1} and EQE_{max} of 18.7%, which can be rationalized by the more balanced electron/hole transporting property of *p*-POSiTPA over *p*-PySiTPA. It is noteworthy that without any light outcoupling enhancement, the peak power efficiency of 47.2 lm W^{-1} for device W2 is close to the highest values of 51.9 lm W^{-1} reported by our group[18b] and 52.7 lm W^{-1} reported by Kido et al.[26] for two-color white PhOLEDs. In addition, devices W1 and W2 show good color stability (Figure 8c and 8d). When the voltage increases from 5 to 8 V, the Commission International de I'Eclairage (CIE) coordinates slightly vary from (0.45, 0.41) to (0.45, 0.42) for device W1, and from (0.42, 0.42) to (0.43, 0.43) for device W2. Affected by the two-color system, the color-rendering index (CRI) of the white devices is not high (58 for device W1 and 60 for device W2).

3. Conclusion

The incorporation of appropriate charge transporting units into the tetraarylsilane skeleton has allowed the realization of a series of wide-bandgap functional materials with high triplet energies, proper HOMO levels and good charge transporting feature. Employing these functional materials results in a simple-structure blue PhOLED that exhibits the highest forward-viewing EQE (up to 22.2%) to date for three-organic-layer FIr6-based blue PhOLEDs. This value is also among the highest for FIr6-based blue PhOLEDs even compared with the four or more than four organic-layer devices. Furthermore, with the introduction of $(fbi)_2Ir(acac)$ as an orange emitter, an all-phosphor warm-white PhOLED has been realized with a peak power efficiency of 47.2 lm W^{-1}, which is close to the highest values ever reported for two-color white PhOLEDs. This work reveals that judicious molecular design of functional materials

is a viable option to realize high-efficiency simple-structure blue and all-phosphor warm-white PhOLEDs, and consequently paves way towards the application of PhOLEDs for displays and lighting sources.

4. Experimental Section

General Information: ^{1}H NMR and ^{13}C NMR spectra were recorded on a MECUYR-VX300 spectrometer. Elemental analyses of carbon, hydrogen, and nitrogen were obtained on a Vario EL III microanalyzer. GC-Mass spectra were collected on a Thermo Trace DSQ II GC/MS. UV-vis absorption spectra were obtained on a Shimadzu UV-2500 spectrophotometer. Photoluminescence (PL) and phosphorescence spectra were measured on a Hitachi F-4500 fluorescence spectrophotometer. A previously reported integrating sphere method was used to determine the PL quantum yields (PLQYs) of the doped films in an absolute PLQY measurement system (Hamamatsus-C10027).[19,27] The films (~50 nm) with 10 wt% FIr6 doped into the host molecules were thermally deposited onto precleaned quartz substrates under high vacuum. The literature value for $Ir(ppy)_3$ [*fac*-tris(2-phenylpyridinato) iridium(III)] doped into CBP (*N,N′*-dicarbazolyl-4,4′-biphenyl) film was utilized to verify against the accuracy of the system.[27] Differential scanning calorimetry (DSC) was carried out on a NETZSCH DSC 200 PC unit under argon with a heating rate of 10 °C min^{-1} from 20 to 300 °C. The glass transition temperature (T_g) was obtained from the second heating scan. Thermogravimetric analysis (TGA) was carried out on a NETZSCH STA 449C instrument under nitrogen with a 10 °C min^{-1} heating rate from 25 to 800 °C. Cyclic voltammetry (CV) was performed with a CHI voltammetric analyzer at room temperature by using the conventional three-electrode configuration which is composed of a platinum working electrode, a platinum wire auxiliary electrode, and an Ag wire pseudoreference electrode. Cyclic voltammograms were recorded at a scan rate of 100 mV s^{-1} with tetrabutylammonium hexafluorophosphate ($TBAPF_6$) (0.1 M) in dichloromethane, tetrahydrofuran or dimethylformamide as the supporting electrolyte, and ferrocenium-ferrocene (Fc^+/Fc) as the internal standard. The onset potential was obtained from the intersection of two tangents drawn at the rising and background current of the cyclic voltammogram.

Device Fabrication and Measurement: The hole-injection material MoO_3, hole-transporting material TAPC, hole/exciton-blocking material Tm3PyPB and electron-transporting material TPBI were commercially available. Commercial ITO (indium tin oxide) coated glass with sheet resistance of 10 Ω per square was used as the starting substrates. Before device fabrication, the ITO glass substrates were precleaned carefully and treated by oxygen plasma for 2 min. All layers were sequentially deposited onto the ITO substrate by vacuum deposition in the vacuum of 10^{-6} Torr. The various device structures were described in the text. *J-V-L* characteristics of the devices were measured with a Keithley 2400 Source meter and a Keithley 2000 Source multimeter equipped with a calibrated silicon photodiode. The EL spectra were measured by JY SPEX CCD3000 spectrometer. The EQE values were calculated according to previously reported methods.[28] All measurements were carried out at room temperature under ambient conditions.

Materials: Bis(4-bromophenyl)(diphenyl)silane (**1**) was prepared according to the literature.[29] Standard procedures are used to dry the solvents. Unless otherwise stated, all reagents were used as received.

*Synthesis of (4-Bromophenyl)(4-iodophenyl)diphenylsilane (**2**)*: n-Butyllithium (3.4 mL, 7.90 mmol, 2.33 M in hexane) was added dropwise to a stirred solution of **1** (3.96 g, 8.00 mmol) in anhydrous THF (80 mL) at −78 °C under argon atmosphere. After stirring at −78 °C for a further 1.5 h, a solution of I_2 (2.54 g, 10.00 mmol) in anhydrous THF (20 mL) was added to give a dark solution. After stirring at −78 °C for 2 h, the mixture was gradually warmed to room temperature under strirring and further reacted overnight. The reaction mixture was quenched with water and then extracted with Et_2O. The combined extracts were washed with 5% aqueous $Na_2S_2O_4$ solution and brine, dried over anhydrous Na_2SO_4, and then concentrated under reduced pressure to provide **2** as a white solid (3.95 g), which was directly used in the next step without further purification.

*Synthesis of {4-[(4-Bromophenyl)(diphenyl) silyl]phenyl}diphenylamine (**3**)*: A mixture of **2** (3.95 g), diphenylamine (1.32 g, 7.80 mmol), CuI (76 mg, 0.40 mmol), and *t*BuOK (1.08 g, 9.60 mmol) in 1,4-dioxane (30 mL) was degassed twice with argon followed by the addition of (±)-*trans*-1,2-diamino-cyclohexane (0.2 mL, 1.60 mmol). After being refluxed for 18 h under argon, the reaction mixture was diluted with brine (60 mL) and extracted with dichloromethane. The combined organic layer was washed with brine and dried over anhydrous Na_2SO_4. After removal of the solvent, the crude product was purified by column chromatography on silica gel using dichloromethane/petroleum (1:5 by vol.) as the eluent to afford a white powder. Yield: 54%. ^{1}H NMR (300 MHz, $CDCl_3$, 25 °C, TMS, δ): 7.57 (d, J = 6.9 Hz, 4H), 7.50–7.40 (m, 8H), 7.37–7.35 (m, 4H), 7.29–7.24 (m, 4H), 7.13 (d, J = 7.5 Hz, 4H), 7.07–7.01 (m, 4H). ^{13}C NMR (75 MHz, $CDCl_3$, 25 °C, δ): 149.20, 147.21, 137.89, 137.14, 136.26, 133.98, 133.67, 131.00, 129.67, 129.31, 127.91, 125.15, 124.59, 123.49, 121.47. MS (EI): m/z 581.0 [M$^+$]. Anal. Calcd for $C_{36}H_{28}BrNSi$ (%): C 74.22, H 4.84, N 2.40. Found: C 74.43, H 4.72, N 2.40.

Synthesis of {4-[Diphenyl(4-pyridin-3-ylphenyl)silyl]phenyl}diphenylamine (p-PySiTPA): A mixture of **3** (2.04 g, 3.50 mmol), pyridin-3-ylboronic acid (0.49 g, 4.00 mmol), $Pd(PPh_3)_4$ (80 mg, 0.07 mmol), and 2 M K_2CO_3 (7 mL, 14.0 mmol) in a mixed solvent of toluene (35 mL) and ethanol (8 mL) was stirred at 100 °C for 48 h under argon. After cooling, the solvent was evaporated under reduced pressure and extracted with dichloromethane. The combined organic phase was washed with brine and dried over anhydrous Na_2SO_4. After removal of the solvent, the crude product was purified by column chromatography on silica gel using ethyl acetate/dichloromethane (1:10 by vol.) as the eluent to provide a white powder. Yield: 54%. ^{1}H NMR (300 MHz, $CDCl_3$, 25 °C, TMS, δ): 8.87 (s, 1H), 8.60 (d, J = 3.6 Hz, 1H), 7.89 (d, J = 8.1 Hz, 1H), 7.71–7.68 (m, 2H), 7.61–7.60 (m, 6H), 7.45–7.35 (m, 9H), 7.29–7.24 (m, 4H), 7.14 (d, J = 7.2 Hz, 4H), 7.06–7.04 (m, 4H). ^{13}C NMR (75 MHz, $CDCl_3$, 25 °C, δ): 149.18, 148.63, 148.34, 147.28, 138.72, 137.27, 137.13, 136.38, 134.75, 134.43, 134.31, 129.68, 129.36, 127.96, 126.51, 125.49, 125.17, 123.65, 123.49, 121.56. MS (EI): m/z 580.4 [M$^+$]. Anal. Calcd for $C_{41}H_{32}N_2Si$ (%): C 84.79, H 5.55, N 4.82. Found: C 85.19, H 5.45, N 4.76.

Synthesis of {4-[[4-(Diphenylphosphoryl)phenyl](diphenyl)silyl]phenyl} diphenylamine (p-POSiTPA): n-Butyllithium (1.8 mL, 4.03 mmol, 2.26 M in hexane) was added dropwise to a stirred solution of **3** (1.96 g, 3.36 mmol) in anhydrous THF (50 mL) at −78 °C under argon atmosphere. After stirring at −78 °C for a further 3 h, chlorodiphenylphosphine (0.86 mL, 4.70 mmol) was added to give a clear, pale-yellow solution. After stirring at −78 °C for 2 h, the mixture was gradually warmed to room temperature under strirring and further reacted overnight. The reaction mixture was quenched with water and then extracted with Et_2O. The combined organic phase was dried over anhydrous Na_2SO_4 and concentrated under reduced pressure. The crude product was dissolved in dichloromethane (20 mL) and then 30% aqueous hydrogen peroxide (8 mL) was added. The mixture was stirred at room temperature for 8 h and then extracted with dichloromethane. The combined organic phase was washed with brine and dried over anhydrous Na_2SO_4. After removal of the solvent, the residue was purified by column chromatography on silica gel using methanol/dichloromethane (1:30 by vol.) as the eluent to afford a white powder. Yield: 32%. ^{1}H NMR (300 MHz, $CDCl_3$, 25 °C, TMS, δ): 7.71–7.62 (m, 8H), 7.56–5.54 (m, 6H), 7.48–7.34 (m, 12H), 7.29–7.24 (m, 4H), 7.13 (d, J = 8.1 Hz, 4H), 7.07–7.01 (m, 4H). ^{13}C NMR (75 MHz, $CDCl_3$, 25 °C, δ): 149.24, 147.14, 137.16, 136.26, 136.11, 133.64, 132.94, 132.12, 131.98, 131.07, 130.96, 129.71, 129.29, 128.54, 128.37, 127.90, 125.15, 124.65, 123.49, 121.37. MS (EI): m/z 703.4 [M$^+$]. Anal. Calcd for $C_{48}H_{38}NOPSi$ (%): C 81.91, H 5.44, N 1.99. Found: C 81.66, H 5.32, N 1.87.

Synthesis of [(Diphenylsilanediyl)bis(4,1-phenylene)]bis(diphenylphosphine) dioxide (SiDPO): Prepared according to the same procedure as *p*-POSiTPA but using bis(4-bromophenyl)(diphenyl)silane (**1**). Yield: 38%. ^{1}H NMR (300 MHz, $CDCl_3$, 25 °C, TMS, δ): 7.71–7.67 (m, 6H),

7.65–7.63 (m, 10H), 7.57–7.53 (m, 8H), 7.50–7.43 (m, 10H), 7.41–7.36 (m, 4H). ^{13}C NMR (75 MHz, $CDCl_3$, 25 °C, δ): 138.23, 135.88, 135.74, 134.44, 133.07, 132.36, 131.69, 130.88, 130.77, 129.77, 128.22, 127.76. MS (EI): m/z 736.5 [M^+]. Anal. Calcd for $C_{48}H_{38}O_2P_2Si$ (%): C 78.24, H 5.20. Found: C 78.06, H 4.93.

Supporting Information

Supporting Information is available from the Wiley Online Library or from the author.

Acknowledgements

The authors are grateful to the National Basic Research Program of China (973 Program 2013CB834805), the National Science Fund for Distinguished Young Scholars of China (51125013) and the Research Fund for the Doctoral Program of Higher Education of China (20120141110029) for financial support.

Received: January 16, 2014
Revised: March 24, 2014
Published online: July 14, 2014

[1] B. W. D'Andrade, S. R. Forrest, *Adv. Mater.* **2004**, *16*, 1585.
[2] T.-H. Han, Y. Lee, M.-R. Choi, S.-H. Woo, S.-H. Bae, B. H. Hong, J.-H. Ahn, T.-W. Lee, *Nat. Photonics* **2012**, *6*, 105.
[3] Z. B. Wang, M. G. Helander, J. Qiu, D. P. Puzzo, M. T. Greiner, Z. M. Hudson, S. Wang, Z. W. Liu, Z. H. Lu, *Nat. Photonics* **2011**, *5*, 753.
[4] M. A. Baldo, D. F. O'Brien, Y. You, A. Shoustikov, S. Sibley, M. E. Thompson, S. R. Forrest, *Nature* **1998**, *395*, 151.
[5] a) L. Xiao, Z. Chen, B. Qu, J. Luo, S. Kong, Q. Gong, J. Kido, *Adv. Mater.* **2011**, *23*, 926; b) S. Gong, Q. Fu, Q. Wang, C. Yang, C. Zhong, J. Qin, D. Ma, *Adv. Mater.* **2011**, *23*, 4956.
[6] a) Y. Tao, C. Yang, J. Qin, *Chem. Soc. Rev.* **2011**, *40*, 2943; b) Y. Tao, Q. Wang, C. Yang, Q. Wang, Z. Zhang, T. Zou, J. Qin, D. Ma, *Angew. Chem., Int. Ed.* **2008**, *47*, 8104; c) S. Gong, X. He, Y. Chen, Z. Jiang, C. Zhong, D. Ma, J. Qin, C. Yang, *J. Mater. Chem.* **2012**, *22*, 2894.
[7] a) S.-J. Su, E. Gonmori, H. Sasabe, J. Kido, *Adv. Mater.* **2008**, *20*, 4189; b) S. Ye, Y. Liu, J. Chen, K. Lu, W. Wu, C. Du, T. Wu, Z. Shuai, G. Yu, *Adv. Mater.* **2010**, *22*, 4167.
[8] K. S. Yook, J. Y. Lee, *Adv. Mater.* **2012**, *24*, 3169.
[9] a) R. J. Holmes, B. W. D'Andrade, S. R. Forrest, X. Ren, J. Li, M. E. Thompson, *Appl. Phys. Lett.* **2003**, *83*, 3818; b) Y. Zheng, S.-H. Eom, N. Chopra, J. Lee, F. So, J. Xue, *Appl. Phys. Lett.* **2008**, *92*, 223301.
[10] a) J. Lee, J.-I. Lee, J.-W. Lee, H. Y. Chu, *Org. Electron.* **2010**, *11*, 1159; b) J. Lee, J.-I. Lee, J. Y. Lee, H. Y. Chu, *Appl. Phys. Lett.* **2009**, *95*, 253304.
[11] a) H.-H. Chou, C.-H. Cheng, *Adv. Mater.* **2010**, *22*, 2468; b) C.-A. Wu, H.-H. Chou, C.-H. Shih, F.-I. Wu, C.-H. Cheng, H.-L. Huang, T.-C. Chao, M.-R. Tseng, *J. Mater. Chem.* **2012**, *22*, 17792.
[12] a) H. Fukagawa, N. Yokoyama, S. Irisa, S. Tokito, *Adv. Mater.* **2010**, *22*, 4775; b) S.-H. Eom, Y. Zheng, E. Wrzesniewski, J. Lee, N. Chopra, F. So, J. Xue, *Org. Electron.* **2009**, *10*, 686.
[13] H. Fukagawa, S. Irisa, H. Hanashima, T. Shimizu, S. Tokito, N. Yokoyama, H. Fujikake, *Org. Electron.* **2011**, *12*, 1638.
[14] X. Ren, J. Li, R. J. Holmes, P. I. Djurovich, S. R. Forrest, M. E. Thompson, *Chem. Mater.* **2004**, *16*, 4743.
[15] A. Chaskar, H.-F. Chen, K.-T. Wong, *Adv. Mater.* **2011**, *23*, 3876.
[16] K. Goushi, R. Kwong, J. J. Brown, H. Sasabe, C. Adachi, *J. Appl. Phys.* **2004**, *95*, 7798.
[17] D. Tanaka, T. Takeda, T. Chiba, S. Watanabe, J. Kido, *Chem. Lett.* **2007**, *36*, 262.
[18] a) S. Gong, Y. Chen, C. Yang, C. Zhong, J. Qin, D. Ma, *Adv. Mater.* **2010**, *22*, 5370; b) S. Gong, Y. Chen, J. Luo, C. Yang, C. Zhong, J. Qin, D. Ma, *Adv. Funct. Mater.* **2011**, *21*, 1168; c) S. Gong, Y. Chen, X. Zhang, P. Cai, C. Zhong, D. Ma, J. Qin, C. Yang, *J. Mater. Chem.* **2011**, *21*, 11197.
[19] A. Endo, K. Suzuki, T. Yoshihara, S. Tobita, M. Yahiro, C. Adachi, *Chem. Phys. Lett.* **2008**, *460*, 155.
[20] P.-I. Shih, C.-H. Chien, F.-I. Wu, C.-F. Shu, *Adv. Funct. Mater.* **2007**, *17*, 3514.
[21] J. Kalinowski, M. Cocchi, D. Virgili, V. Fattori, J. A. G. Williams, *Adv. Mater.* **2007**, *19*, 4000.
[22] S.-J. Su, Y. Takahashi, T. Chiba, T. Takeda, J. Kido, *Adv. Funct. Mater.* **2009**, *19*, 1260.
[23] S.-y. Takizawa, V. A. Montes, P. Anzenbacher, , Jr., *Chem. Mater.* **2009**, *21*, 2452.
[24] a) V. Sivasubramaniam, F. Brodkorb, S. Hanning, H. P. Loebl, V. van Elsbergen, H. Boerner, U. Scherf, M. Kreyenschmidt, *J. Fluorine Chem.* **2009**, *130*, 640; b) S. Schmidbauer, A. Hohenleutner, B. König, *Adv. Mater.* **2013**, *25*, 2114.
[25] W.-S. Huang, J. T. Lin, C.-H. Chien, Y.-T. Tao, S.-S. Sun, Y.-S. Wen, *Chem. Mater.* **2004**, *16*, 2480.
[26] H. Sasabe, J.-i. Takamatsu, T. Motoyama, S. Watanabe, G. Wagenblast, N. Langer, O. Molt, E. Fuchs, C. Lennartz, J. Kido, *Adv. Mater.* **2010**, *22*, 5003.
[27] Y. Kawamura, K. Goushi, J. Brooks, J. J. Brown, H. Sasabe, C. Adachi, *Appl. Phys. Lett.* **2005**, *86*, 071104.
[28] S. R. Forrest, D. D. C. Bradley, M. E. Thompson, *Adv. Mater.* **2003**, *15*, 1043.
[29] L.-H. Chan, R.-H. Lee, C.-F. Hsieh, H.-C. Yeh, C.-T. Chen, *J. Am. Chem. Soc.* **2002**, *124*, 6469.